Hybrid 2D and 3D Frameworks Based on ε-Keggin Polyoxometallates: Experiment and Simulation

Anne Dolbecq,*[a] Caroline Mellot-Draznieks,[a] Pierre Mialane,[a] Jérôme Marrot,[a] Gérard Férey,[a] and Francis Sécheresse[a]

Keywords: Molybdenum / Organic–inorganic hybrid materials / Polyoxometallates / Simulation

The ε-Keggin polyoxomolybdate {ε-$PMo^{V}_{8}Mo^{VI}_{4}O_{40-x}(OH)_x$-$M_4$} is a versatile building unit, with M being either a Zn^{II} or a La^{III} capping ion located at the vertices of a slightly distorted tetrahedron. The charge of the Keggin unit depends on the number of protonated oxo bridging ligands, which has been shown to vary from 0 to 5. The Keggin entity can thus be either an anion (M = Zn, x = 0) or a cation (M = La, x = 3–5). The Zn derivative has been generated in situ by hydrothermal synthesis and forms a 2D material built from the connection of the cations by 4,4′-bipyridine ligands linked to the capping Zn^{II} ions. The reaction of the chloride salt of the La derivative with di-, tri- and tetrasubstituted benzenecarboxylate ligands has allowed us to isolate 2D and 3D materials. The 3D materials seem to be the first examples of hybrid open frameworks based on Keggin building blocks. The 3D framework built from the connection of ε-Keggin units by trimesate ions exhibits tunnels filled only by water molecules, which can be partly removed and reintroduced at room temperature. Besides these experimental results, simulation has allowed us to generate two virtual hybrid structures derived from those of known silicates by replacing the Si ions by hypothetical ε-Keggin cations and the *O*-bridging ligands by terephthalate ions, thus showing that 3D frameworks with large pores can be envisioned in the chemistry of hybrid organic–inorganic materials based on ε-Keggin units and motivating further experimental investigations.

Introduction

Metal–organic frameworks[1] constitute a recent class of materials with open architectures built from metal ions linked together by organic bridging ligands, most of the time carboxylate ions.[2] These compounds have attracted much interest because of their potential applications in catalysis, gas storage and separation. Their structures can be classified according to the dimensionality of the inorganic network.[3] The largest family contains metal–organic frameworks with discrete inorganic building blocks. Two factors determine the geometry and the size of the cavities, namely the symmetry and size of the molecular units and the nature of the organic ligand. For example, Yaghi et al. have shown that the volume of the cavities increases dramatically when the bridging organic ligand is lengthened.[4] Another way to expand the lattice, known as "scale chemistry",[5] is to increase the size of the inorganic building blocks, which are so far limited to a small number of metal ions. We have recently reported the synthesis of a novel polyoxocation, $[\varepsilon\text{-}PMo^{V}_{8}Mo^{VI}_{4}O_{36}(OH)_4\{La(H_2O)_4\}_4]^{5+}$, which is a mixed-valence ε-Keggin-type polyoxometallate (POM) core capped by four lanthanum ions located at the vertices of a slightly distorted tetrahedron.[6] The La^{III} ions are connected to the molybdenum ions by three triply bridging oxygen atoms and their coordination sphere is completed by disordered water molecules. The overall symmetry of the polyoxocation is tetrahedral. Two examples of transition metal cations (Zn^{II}, Ni^{II}) capping reduced ε-Keggin cores have also been reported.[7] The water molecules bound to transition metal or rare-earth cations capping the POM core can be potentially substituted by N- or O-donor ligands, which opens the way to the design of a new family of hybrid organic–inorganic materials. We have recently obtained the first members of this family, namely two 1D materials formed by the connection of the POMs by squarate or glutarate ligands, respectively.[8] Nevertheless, owing to the overall tetrahedral symmetry of the inorganic cation, 3D materials can be envisioned, which can lead eventually to porous frameworks. We describe in this paper our first results in the synthesis of 2D and 3D frameworks with the ε-Keggin building unit, synthesised by two different ways, namely hydrothermal techniques, which have led to $Na(C_{10}H_{10}N_2)[\varepsilon\text{-}PMo_{12}O_{40}Zn_4(H_2O)_2(C_{10}H_8N_2)_3]\cdot 10H_2O$ (**1**), and standard bench conditions, which have allowed us to isolate $[\varepsilon\text{-}PMo_{12}O_{35}(OH)_5La_4(C_8H_4O_4)_3]\cdot 41H_2O$ (**2**), $[\varepsilon\text{-}PMo_{12}O_{35}(OH)_5\{La(H_2O)_3\}_4(C_9H_3O_6)_2]\cdot 44H_2O$ (**3**) and [ε-

[a] Institut Lavoisier, IREM, UMR 8637, Université de Versailles Saint-Quentin,
45 Avenue des Etats-Unis, 78035 Versailles cedex, France
Fax: +33-139254381
E-mail:dolbecq@chimie.uvsq.fr
Supporting information for this article is available on the WWW under http://www.eurjic.org or from the author.

$PMo_{12}O_{37}(OH)_3\{La(H_2O)_4\}_4(C_{10}H_2O_8)]\cdot 24H_2O$ (**4**). The synthetic routes to obtain the different compounds described in this paper are summarised in Figure 1. Besides these experimental results, we also report here the simulation of two phases built from the connection of a hypothetical ε-Keggin core, capped by pentacoordinate transition metal ions, by a rigid dicarboxylate ligand − the terephthalate ligand − in order to demonstrate the potentiality of this molecular building block for the design of hybrid organic–inorganic materials with large pores.

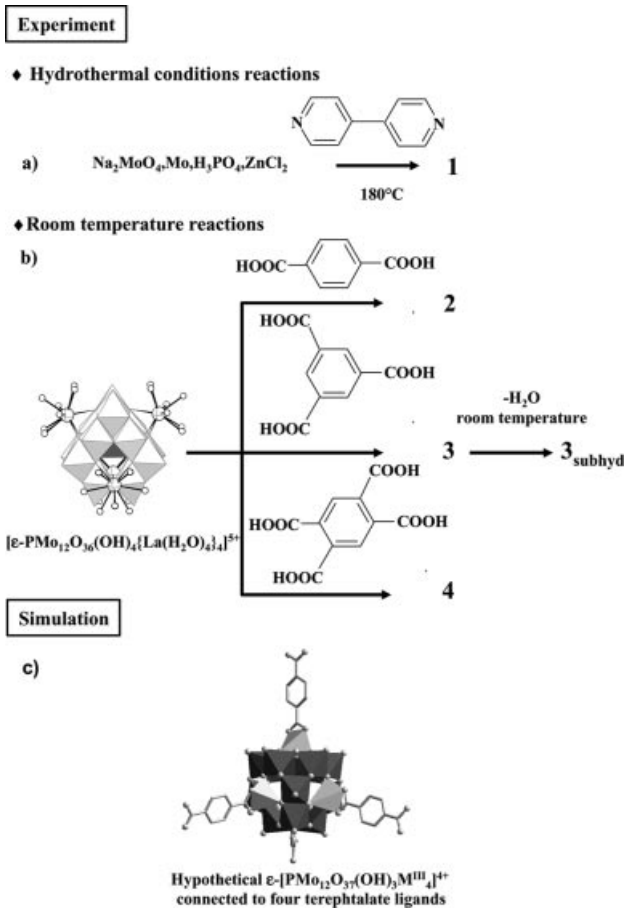

Figure 1. The synthetic conditions used to obtain a) **1** in a hydrothermal "one-pot" synthesis and b) **2**, **3** and **4** from the $[\varepsilon\text{-}PMo_{12}O_{36}(OH)_4\{La(H_2O)_4\}_4]^{5+}$ precursor. Note that for $[\varepsilon\text{-}PMo_{12}O_{36}(OH)_4\{La(H_2O)_4\}_4]^{5+}$ the four water molecules are disordered on the lanthanum ions; c) polyhedral representation of the hypothetical ε-Keggin ion with pentahedral capping transition ions used for the simulation.

Results and Discussion

Synthesis

The synthesis of the hybrid materials with ε-Keggin building units was performed according to two different procedures: the first one exploits hydrothermal conditions and the second one is based on the substitution of water molecules bound to the lanthanum ions of the inorganic precursor by carboxylate groups of the organic ligand (Figure 1). We first chose Zn^{II} ions as capping transition metal ions in hydrothermal reactions because of their ability to adopt low coordination numbers and thus favour the 1:2 POM:ligand stoichiometry. 4,4′-Bipyridine was selected as ligand because it is neutral and thus it should have a greater affinity for the most probable anionic ε-Keggin core capped with divalent Zn ions than the terephthalate ligand. Single crystals of $Na(C_{10}H_{10}N_2)[\varepsilon\text{-}PMo_{12}O_{40}Zn_4(H_2O)_2(C_{10}H_8N_2)_3]\cdot 10H_2O$ (**1**) were obtained from the reaction of a mixture of Na_2MoO_4, Mo as reducing agent, H_3PO_4, $Zn(CH_3COO)_2$ and 4,4′-bipyridine in water adjusted to pH 6.5, and heated at 180 °C. The ε-Keggin core capped with Zn^{II} ions is generated in situ and connects three different neutral bidentate ligands to generate a 2D material. Although the synthetic conditions are quite different, especially the Zn:ligand ratio and the nature of the precursors, the structure of **1** (see below) is close to that of a 2D material reported recently.[7b]

Despite numerous attempts, single crystals of $[\varepsilon\text{-}PMo_{12}O_{35}(OH)_5La_4(C_8H_4O_4)_3]\cdot 41H_2O$ (**2**) of suitable quality for X-ray diffraction could not be obtained, and only microcrystalline powders were formed by slow addition of an aqueous solution of terephthalic acid to a methanolic solution of $[\varepsilon\text{-}PMo_{12}O_{36}(OH)_4\{La(H_2O)_{2.5}Cl_{1.25}\}_4]\cdot 27H_2O$.[6] Elemental analysis indicates that the stoichiometry of the hybrid compound is one ε-Keggin ion for three terephthalate ligands. The structure of **2** is thus certainly very close to that of **1**, with terephthalate ligands in place of bipyridine and La^{III} ions replacing Zn^{II} ions, as also suggested by the similarity of their experimental powder diffraction patterns (Figure 3, b). However, the poor quality of the experimental diagram of **2** prevents any further investigation of the structure.

Single crystals of $[\varepsilon\text{-}PMo_{12}O_{35}(OH)_5\{La(H_2O)_3\}_4(C_9H_3O_6)_2]\cdot 44H_2O$ (**3**) were grown by slow evaporation, at room temperature, of a CH_3OH/H_2O solution containing the chloride salt of the ε-Keggin precursor and a stoichiometric amount of trimesate ions. The determining factors for the crystallisation process are the CH_3OH/H_2O ratio, the pH of the trimesate solution and the stoichiometry of the reaction. Compound **3** rapidly loses water at room temperature to give $\mathbf{3_{subhyd}}$. Single crystals of $[\varepsilon\text{-}PMo_{12}O_{37}(OH)_3\{La(H_2O)_4\}_4(C_{10}H_2O_8)]\cdot 24H_2O$ (**4**) were obtained in a similar manner except that a pure water solution was used instead of a mixture of CH_3OH and H_2O. In the presence of an excess of ligand, and/or if the pH is too high, only microcrystalline powders precipitate.

The infrared spectra of **1**, **2**, $\mathbf{3_{subhyd}}$ and **4** are very similar in the 970–500 cm^{-1} region, where characteristic Mo=O and Mo–O vibrations are found. The bands of **2**, $\mathbf{3_{subhyd}}$ and **4** in the 1650–1350 cm^{-1} domain are characteristic of the O–C–O vibrations of the coordinated ligand.

Structure of $Na(C_{10}H_{10}N_2)[\varepsilon\text{-}PMo_{12}O_{40}Zn_4(H_2O)_2(C_{10}H_8N_2)_3]\cdot 10H_2O$ (1)

The ε-Keggin unit is similar to the building unit encountered in the 1D solids with glutarate and squarate ligands,[8]

Table 1. Ranges and mean bond lengths [Å] within the POM core in **1**, **3** and **4**.

	1	**3**	**4**
P–O	1.529(15)–1.541(10) [1.534]	1.551(6)–1.555(6) [1.553][a]	1.540(6)–1.576(6) [1.559]
Mo–O_a[b]	2.515(14)–2.586(14) [2.528]	2.473(6)–2.647(6) [2.553]	2.434(5)–2.682(5) [2.541]
Mo–$O_{b,c}$[b] *Short*	1.872(11)–2.043(10) [1.956]	1.824(7)–2.027(6) [1.951]	1.794(5)–2.032(5) [1.948]
Long[c]		2.062(7)–2.083(6) [2.074]	2.014(6)–2.094(5) [2.049]
Mo–O_d[b]	1.643(12)–1.683(13) [1.665]	1.676(7)–1.688(7) [1.681]	1.651(6)–1.708(6) [1.675]
Mo^V–Mo^V	2.573(3)–2.614(3) [2.593]	2.5774(12)–2.5983(19) [2.585]	2.5637(11)–2.6215(11) [2.589]
Mo···Mo[d]	2.882(3)–2.869(3) [2.875]	3.1326(13) [3.133]	3.1476(11)–3.1501(10) [3.149]

[a] Mean values are indicated in square brackets. [b] O_a refers to an oxygen atom of the central cavity bound to the phosphorus atom; O_b and O_c refer to bridging oxygen atoms; O_d refers to a terminal oxygen atom. [c] Mo–O distances for O atoms bridging two Mo atoms of the Keggin core with two corresponding Mo–O distances longer than 2.0 Å. [d] Mo···Mo distances between 2.80 and 3.20 Å.

and in the 3D materials **3** and **4** (see below) except that the Mo^V and Mo^{VI} ions are not all localised, as observed previously. Indeed, while valence bond calculations[9] (Table S1, Supporting Information) indicate clearly that Mo1, Mo6 and Mo7 are Mo^V ions, in agreement also with their short intermetallic Mo–Mo bonds (Table 1), the four Mo^{VI} ions and four Mo^V ions remaining are delocalised over eight centres. The Mo–Mo distances for these ions (Table 1) are intermediate between Mo^V–Mo^V (ca. 2.6 Å) and Mo^{VI}···Mo^{VI} bonds (ca. 3.2 Å). The $[\varepsilon\text{-}PMo^V_8Mo^{VI}_4O_{40}]^{11-}$ core is stabilized by four Zn^{II} capping ions and this entity is thus formally anionic. Due to the smaller ionic radii of the Zn^{II} ions compared to the La^{III} ions, and consequently shorter Zn–O distances (Table 2 and Table S2 in the Supporting Information), the volume occupied by the ε-Keggin core is far smaller when it is capped by Zn^{II} ions. A rough estimation, using the mean distance between the central phosphorus atom and the atoms of the ligands L coordinated to the Zn^{II} or La^{III} ions as the radius of a sphere, leads to a volume of 775 $Å^3$ for the Zn derivative ($d_{P\cdots L} \approx 5.7$ Å) and 1630 $Å^3$ for the La derivative ($d_{P\cdots L} \approx 7.3$ Å).

Table 2. Ranges and mean bond lengths [Å] for the Zn–O, Zn–N bonds in **1** and the La–O and C–O bonds in **3** and **4**.

	1
Zn–O[a]	1.897(14)–2.268(18) [2.036]
Zn–N	2.014(11)–2.150(16)(2) [2.068]
	3
La–O(POM)	2.442(7)–2.625(8) [2.551]
La–O(H_2O)	2.500(11)–2.598(8) [2.563]
C–O	1.249(13)–1.308(14) [1.270]
	4
La–O(POM)	2.452(5)–2.676(5) [2.556]
La–O(H_2O)	2.499(6)–2.758(12) [2.610]
C–O	1.207(10)–1.293(10) [1.254]

[a] Mean values are indicated in square brackets.

Three different coordination modes are encountered in **1**. Thus, Zn1 is pentacoordinate, being bound to three oxygen atoms of the ε-Keggin core and two nitrogen atoms of two 4,4′-bipyridine ligands (Figure 2), Zn2 is bound to three oxygen atoms of the Keggin core, one nitrogen atom of a bipyridine ligand and two additional water molecules, and is thus hexacoordinate, and Zn3 only bears one extra ligand, i.e. a bypiridine molecule, and is tetracoordinate (Figure 2). In the (*a*,*b*) plane, one ε-Keggin unit is connected to four adjacent units through four bipyridine molecules linked to Zn1 ions, thus forming a double chain (Figure 3, a). These double chains stack along the *c* axis and are connected to neighbouring ones by bipyridine ligands linked to the Zn2 and Zn3 ions, thus forming a double plane. Intersecting tunnels along the *b* and *c* directions are generated, however the adjacent planes interpenetrate (Figure 3, a) and the material does not exhibit any porosity. Furthermore, disordered sodium ions and free protonated bipyridine ions are found as counterbalancing cations.

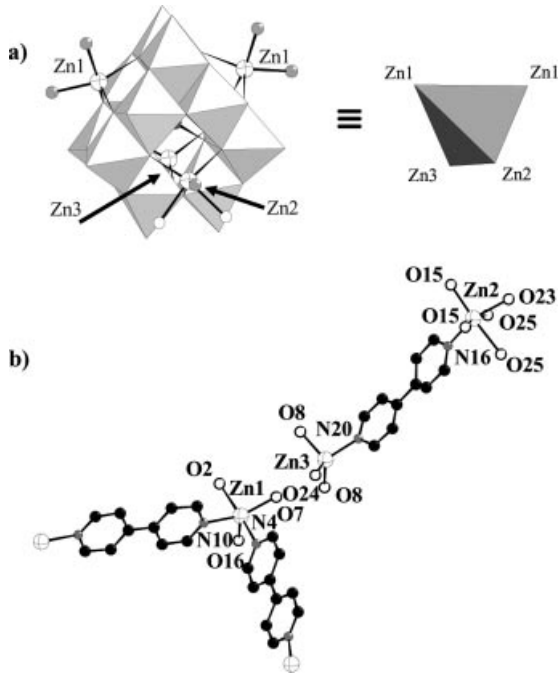

Figure 2. a) Representation of the building unit in **1**, showing the three different coordination modes of the Zn^{II} capping ions and its overall tetrahedral symmetry; b) labelling scheme of the Zn^{II} centres and their ligands.

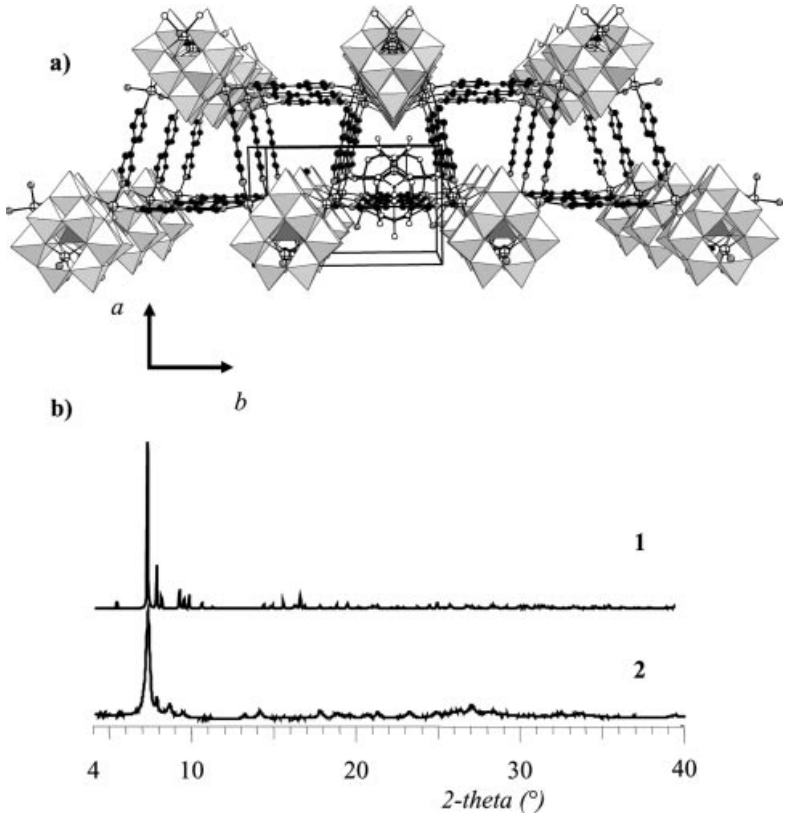

Figure 3. a) View of the double chains in the (*a*,*b*) plane formed by the connection of ε-Keggin units by bipyridine ligands; the connection along the *c* axis ensure the formation of planes. The position of an ε-Keggin cation (ball and stick representation) belonging to an adjacent double plane is also shown. Non-coordinated water molecules and bipyridinium counterions have been omitted for clarity. b) Comparison of the simulated powder pattern of **1** and the experimental powder pattern of **2**.

Structure of $[\varepsilon\text{-}PMo_{12}O_{35}(OH)_5\{La(H_2O)_3(C_9H_3O_6)_2\}]\cdot 44H_2O$ (3)

Crystals of **3** rapidly become amorphous when left in air. X-ray analysis was therefore performed on a single crystal of **3** sealed in a capillary tube. Compound **3**, which exhibits a three-dimensional structure, crystallises in the non-centrosymmetric space group $P2_12_12$. One organic ligand connects three different polyoxocations through La–O bonds, two carboxylate groups adopt a chelating mode while one pendent oxygen atom (O26) remains in the third one (Figure 4, a). The quite short C–O distance [C9–O26 = 1.258(14) Å] of the pendent group indicates that this group is non-protonated. This bonding mode of the trimesate ligand has been encountered a few times.[10] Each lanthanum ion bears three additional water molecules, and the lanthanum ion connected to the bridging carboxylate group (La1) is also connected to another trimesate ligand, therefore the La1 ions are enneacoordinate whereas the La2 ions are only octacoordinate. The geometrical features within the polyoxometallate core are slightly affected by the coordination to organic ligands. As observed for the polymeric structure with squarate and glutarate ions,[8] among the twelve Mo ions, eight Mo^V ions form Mo–Mo bonds ($d_{Mo-Mo} \approx 2.6$ Å, Table 1) while the remaining four are Mo^{VI} centres ($d_{Mo\cdots Mo} \approx 3.2$ Å). Valence bond calculations (Table S1, Supporting Information) confirmed the oxidation state of the Mo ions

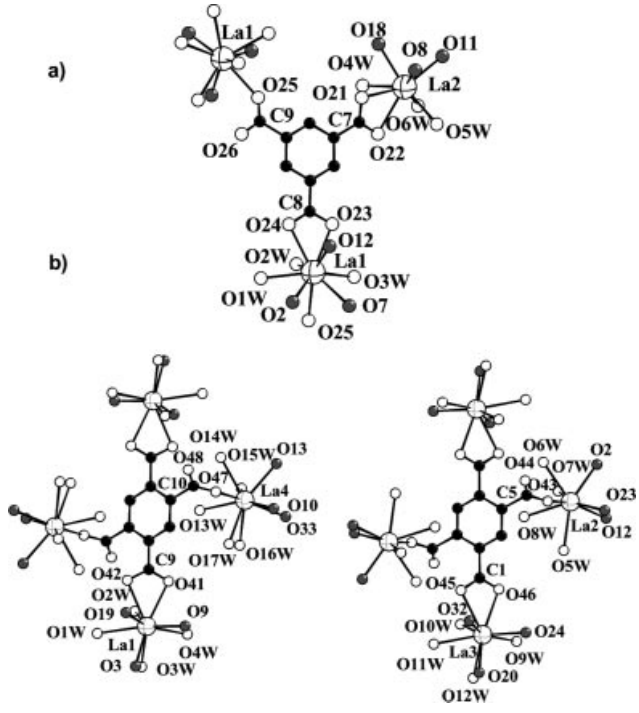

Figure 4. Bonding mode of a) the trimesate ligand in **3** and b) the pyromellitic ligands in **4**; the oxygen atoms bound to the POM core are represented as grey spheres.

and allowed us to localise four protons on bridging oxygen atoms of the POM core. In order to respect the electroneutrality, one additional proton is assumed to be delocalised over the four remaining μ_2-oxygen atoms of the POM. Indeed, it is well known that the basicity of a Keggin polyoxomolybdate increases when it is reduced, and the doubly bridging oxygen atoms are the preferred protonation sites.[11] The connection of the polyoxocations by the tridentate ligands generates a neutral 3D framework with 1D channels running along the *c* axis (Figure 5). The channels have rectangular free apertures of 6.1 × 7.2 Å, as estimated from the interatomic distances between atoms delimiting the channels and taking into account their van der Waals radii. These channels are filled with clusters of disordered water molecules that form intricate hydrogen bonds with other water molecules of the clusters and the oxygen atoms of the polyoxocation.

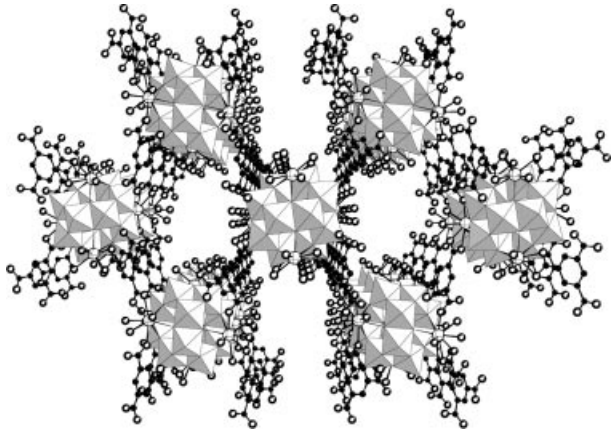

Figure 5. Perspective view of the 3D structure of **3** showing the channels along the *c* direction. Non-coordinated water molecules have been omitted for clarity.

Structure of $[\varepsilon\text{-}PMo_{12}O_{35}(OH)_5\{La(H_2O)_3\}_4(C_{10}H_2O_8)]\cdot 24H_2O$ (4)

Compound **4** crystallises in the centrosymmetric $P\bar{1}$ space group. The asymmetric unit contains a POM polyoxocation and two halves of the organic ligand, in agreement with the 1:1 stoichiometry. Each ligand is bound to four lanthanum ions from four distinct POMs (Figure 4, b). Like in **3**, there are two different connecting modes of the carboxylate groups: two are chelating and two are only monodentate C–O groups. The O–C–O groups are almost perpendicular to the plane of the organic molecule. La2 and La1 are connected to monodentate C–O groups, and La2 bears four additional water molecules in addition to the three oxygen atoms of the POM and is thus octacoordinate while La1 has a supplementary water molecule and is nonacoordinate. La3 and La4 are bound to chelating carboxylate groups and are both nonacoordinated. The geometrical features within the POM are similar to those in **3** (Table 1). The connection of one POM to the organic ligands by La–O–C bonds generates a 3D material that contains small channels running along the *b* axis that are filled, as in **3**, by disordered water molecules (Figure 6).

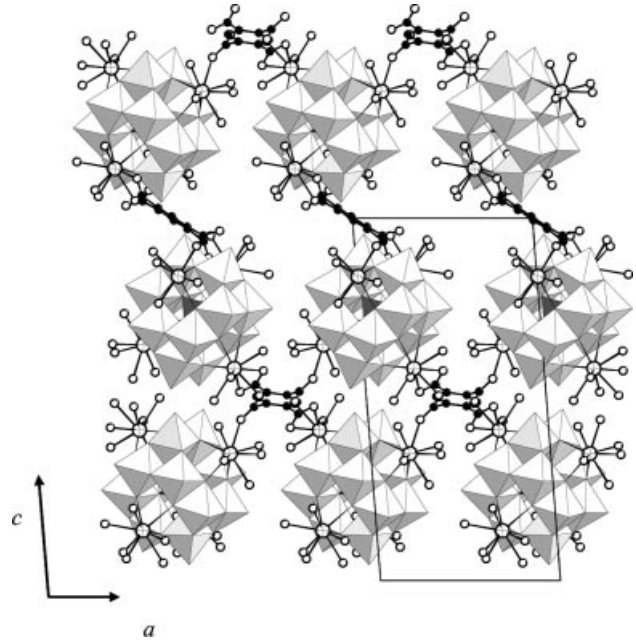

Figure 6. View of the 3D structure of **4** along the *b* axis. Non-coordinated water molecules have been omitted for clarity.

Subhydrate of 3

The stability of **3** was investigated first by a simple treatment at room temperature. The X-ray powder diffraction pattern of freshly filtered, ground crystals of **3** does not exactly fit the calculated powder pattern obtained from the single-crystal X-ray diffraction experiment (Figure 7). Indeed, the first peak is observed for a 2θ value of 6.10° (Figure 7, d), while the first peak in the calculated powder pattern is obtained for a 2θ value of 5.93° (Figure 7, b). This powder pattern progressively evolves with time; the first peak broadens and shifts toward higher 2θ values, while the position of the other ones remains approximately unchanged (Figures 7, e and f). No further change is observed after a few hours at room temperature, indicating that the partial dehydration of **3** is achieved to give $\mathbf{3_{subhyd}}$. When a drop of water is added to the powder sample of $\mathbf{3_{subhyd}}$, the X-ray powder pattern changes and the position of the first peak (Figure 7, c) now matches the position of the first peak in the calculated powder pattern (Figure 7, a). This experiment shows that the dehydration at room temperature is reversible.

Despite the poor quality of the experimental X-ray powder pattern, we tried to simulate the structure of the dehydrated sample $\mathbf{3_{subhyd}}$ by lattice energy minimisations[20] to reproduce the positions of the experimental diffraction peaks. This simulation allowed us to calculate the cell parameters of the dehydrated sample and showed that the contraction mainly affects the *a* parameter.[12] The channels shrink upon dehydration, in agreement with a hydrophobic

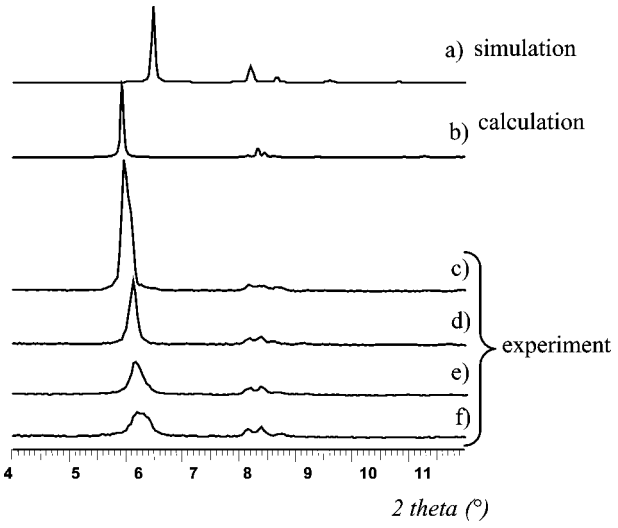

Figure 7. a) Simulated diffraction powder pattern of $\mathbf{3}_{\mathbf{subhyd}}$; b) calculated diffraction powder pattern from the single-crystal X-ray diffraction structure of **3**. Experimental diffraction powder pattern: c) $\mathbf{3}_{\mathbf{subhyd}}$ to which a drop of water has been added, d) **3** freshly filtered (t = 5 min), e) t = 30 min, f) t = 2 h.

character, as a consequence of the presence of aromatic rings on the channel walls. The difference between the volumes of **3** and $\mathbf{3}_{\mathbf{subhyd}}$ (reduction of 12%) leads to an estimated number of water molecules lost by the dehydration at room temperature of 17, assuming that a hydrogen-bonded water molecule occupies a volume of 40 Å^3. The thermogravimetric analysis (TGA) curve performed on $\mathbf{3}_{\mathbf{subhyd}}$ (Figure S1) shows an initial weight loss of 16.0% (calcd. 16.1) attributable to the loss of 32 water molecules trapped within the channels. The second weight loss of 9.6% (calcd. 9.4) corresponds to the loss of water molecules bound to the lanthanum ions and to the formation of oxides. This is in agreement with the following formula [ε-$PMo_{12}O_{35}(OH)_5$-$\{La(H_2O)_3\}_4(C_9H_3O_6)_2$]·$32H_2O$ for $\mathbf{3}_{\mathbf{subhyd}}$, while elemental analysis is more in favour of 27 hydration water molecules (see Experimental Section).

The presence of tunnels filled only with water molecules motivated a measurement of the surface area. Nevertheless, after activation of the sample at 70 °C a BET nitrogen adsorption measurement performed on $\mathbf{3}_{\mathbf{subhyd}}$ revealed a low surface area (ca. 14 $m^2 g^{-1}$), thus confirming the X-ray thermodiffractometry experiment, which shows that the structure collapses. At variance with the dehydration at room temperature and ambient pressure, the dehydration under vacuum is therefore irreversible.

The description of the four hybrid organic–inorganic materials **1**–**4** based on the ε-Keggin unit shows the complexity of these systems. However, an important feature arises from this study: Keggin ions can be used as inorganic bricks to build up hybrid open frameworks. To the best of our knowledge, it indeed seems that this has been found here for the first time. This is probably due to the possibility for ε-Keggin ions to be tetrahedrally decorated by four cations, which act as points of anchorage for linking organic species, and also means that the serendipity which often governs the POM:ligand stoichiometry can be surpassed by the introduction of computer prediction of possible Keggin-based hybrid frameworks. In order to tentatively rationalise what family of open frameworks compounds could be envisioned, the following section describes our first simulation results.

Computational Section

In the current search for new and interesting hybrid open frameworks, the predictability of the framework architecture and its resulting dimensionality are essential. It is highly valuable to consider how systematic approaches may be computationally developed for producing new hybrid frameworks, with the desire of developing virtual libraries that might be accessible through synthesis. With this in mind, some of us (C.M-D, G.F.), have made important efforts to introduce a computational prediction of crystal structures using the concept of building units.[5] The resulting AASBU method (Automated Assembly of Secondary Building Units)[13] was initially devoted to inorganic structures, but the applicability of the method in the realm of hybrid solids has been demonstrated recently.[14] The key feature of the method lies in the use of pre-defined organic and inorganic building units together with pre-defined connection points on each type of unit. The simulations explore their assembly in 3D space through a cascade of simulated annealing and minimisation steps. Indeed, this simulation approach focuses on the capacity of the organic and inorganic sub-units to generate infinite networks, resulting in a list of candidate periodic crystalline arrangements and their respective space group, cell parameters and atomic coordinates.

One of the key points for the success of the method is the knowledge of the chemical conditions associated with the existence of a given building block in the solution. In the same way as we demonstrated the existence of Cr_3–μ_3-O clusters,[14c] the [ε-$PMo^{V}_8Mo^{VI}_4O_{36}(OH)_4$-$\{La(H_2O)_4\}_4$]$^{5+}$ Keggin ion has been characterised in solution.[6] Its recurrence in experimental crystal structures is a clear evidence that the Keggin ion may be regarded as a building unit, the condensation of which with an appropriate organic linker might lead to a whole series of hybrid infinite networks. This section presents an attempt to produce hybrid infinite networks computationally by assembling Keggin inorganic units with a carefully chosen organic counterpart and to demonstrate the capacity of the simulation approach for generating hybrid open-framework candidates that are all built from the same pre-defined Keggin ion and organic ligand, in other words hybrid polymorphs.

In the present computational work, we selected terephthalic acid as a good candidate to generate hypothetical Keggin-based hybrid structures owing to its rigid carbon skeleton and its simple bidentate character. The use of 4,4′-bipyridine would have led to similar results. The isolated Keggin ion offers four anchorage points to the carboxylate function through its four capping M ions, which are placed

at the corners of a virtual tetrahedron (M is chosen here as a trivalent M^{III} ion). The Keggin–terephthalic acid linkages therefore lead to pentacoordinate M^{III} cations, where each M cation is coordinated to three oxygen atoms of the Keggin ion and two oxygen atoms of the carboxylate ligand. This ε-Keggin cation, with four pentacoordinate capping transition metal ions, is currently a hypothetical ion which has never been isolated but which is chosen here in order to simplify the calculations. Interestingly, considering that each Keggin ion may connect to four terephthalic acids in the four directions of a tetrahedron (Figure 1), the infinite connection of alternating Keggin ions and terephthalic acids is deemed to lead to four-connected networks similar to those observed in dense silicates such as quartz or microporous silicates such as zeolites,[15] all of which contain corner-sharing SiO_4 tetrahedra.

In the present work, the simulation of two candidate hybrid structures is presented. Using the above analogy with silicates, we assembled the Keggin ion and terephthalate ligands in 3D space to simulate two upper hybrid analogues which correspond to the quartz-α and LTA augmented nets.[16] Indeed, according to O'Keeffe et al., each augmented net possesses the same topology as two existing silicates or aluminosilicates: quartz-α ($P3_22_1$, a = 4.90 Å, c = 5.40 Å) and zeolite LTA ($Fm\bar{3}c$, a = 24.61 Å). Both frameworks result from the corner-sharing arrangement of SiO_4 tetrahedra. The crystallographic position of the Si atoms of the silicate structures is indicative of the required positioning of each Keggin ion centre, while the crystallographic position of the oxygen atoms is indicative of the required positioning of the centre of the organic molecule ensuring the linkage between two adjacent Keggin ions. Indeed, this construction process fully uses the analogy between the Si–O–Si linkages typically found in silicates and the metal–ligand–metal linkages found in metal–organic frameworks. The important size of the Keggin ion and of the organic molecule in comparison with that of Si and O atoms requires an extension of the size of each unit cell. The cell size of quartz-α increases to $a \approx 30$ Å, while that of zeolite LTA to more than 130 Å, keeping the Si and O atoms at the same crystallographic positions. In a subsequent step, the replacement of each independent Si and O atom by a Keggin ion and an organic ligand, respectively, was performed in each unit cell, resulting in two hybrid crystal structures with the same chemical composition [ε-$PMo_{12}O_{37}(OH)_3(M^{III})_4](O_2C\text{-}C_6H_4\text{-}CO_2)_2$. In some cases, these steps required a lowering of the initial symmetry. As a final step, the two hybrid crystal structures were submitted to lattice energy minimisations by allowing the atomic positions and the cell parameters to relax. Short-range interactions were calculated with the UFF forcefield.[17] The electrostatic contribution was calculated with an Ewald summation by using partial charges obtained from the charge equilibration method.[18] The simulations were performed using the Cerius2 suite of software[19] on an Octane SGI R12000 workstation operating at 300 MHz.

Energy-minimised structures of the quartz-type and of the LTA-type are shown in Figures 8 and 9, respectively, together with their simulated X-ray powder diffraction pattern (Cu-K_α respectively). The hybrid LTA-type Keggin dicarboxylate converged with cell parameters of a = 119.25 Å, while that of the minimised quartz-type Keggin-dicarboxylate possesses cell parameters of a = 25.93 Å and c = 24.20 Å. The quartz-type structure (Figure 8) can be described as a 3D network of Keggin cations connected by terephthalate ligands to form exclusively distorted 6-rings, directly emanating from the quartz topology. Hence it is a

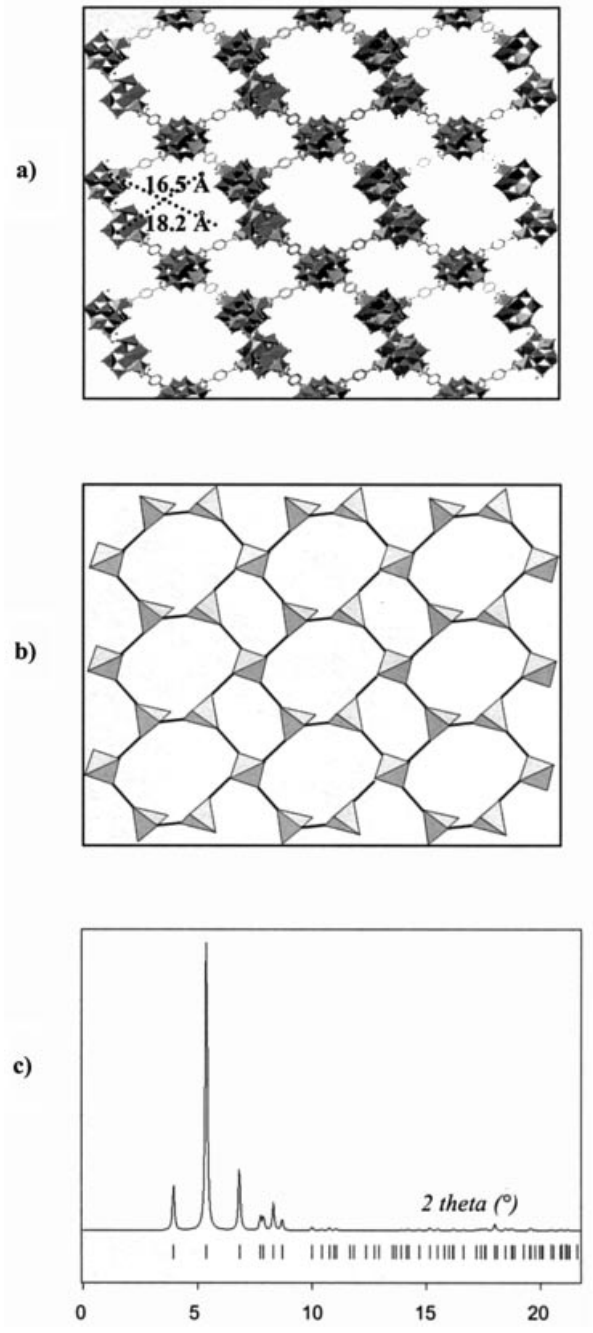

Figure 8. a) Projection along the a axis of the energy minimised structure of the quartz-α type; b) schematic view with ε-Keggin units represented by tetrahedra and terephthalate ligands by rods; c) simulated X-ray powder diffraction pattern (Cu-K_α).

porous hypothetical structure which forms channels delimited by six Keggin ions with accessible diameters of 16.5×18.3 Å. The LTA-type structure (Figure 9) contains small cages (sodalite-type cages) made of 6-rings of Keggin ions and 4-rings, visible at the centre of Figure 9. Their assembly along each direction generates a bigger cage (here called supercage), made of 4-, 6- and 8-rings, four of which are visible at each corner of Figure 9. These supercages communicate with one another through 8-rings, the connection of which generates channels with larget dimensions (ca. 40 Å of diameter from one terephthalate to the opposite one). The inner diameter of the supercage is around 84 Å. These lattice energy calculations are a preliminary study to a more extended work on the relative stabilities of Keggin-containing hybrid frameworks. We believe that these two hypothetical structures are indicative of the viability of such open-framework architectures.

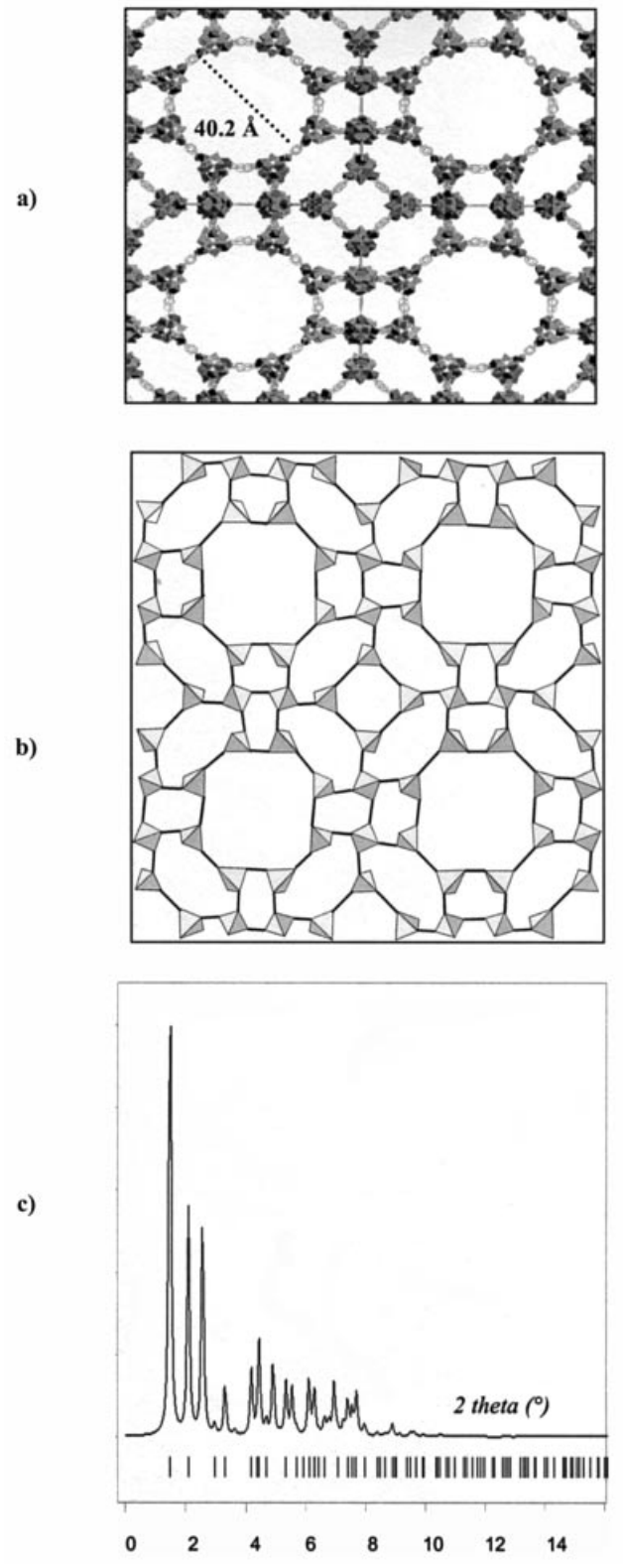

Figure 9. a) Projection along the *c* axis of the energy minimised structure of the zeolite LTA type, b) schematic view with ε-Keggin units represented by tetrahedra and terephthalate ligands by rods, c) simulated X-ray powder diffraction pattern (Cu-K_α).

Conclusions

This study demonstrates that it is possible to build extended frameworks containing a polyoxomolybdate building unit, under mild or hydrothermal conditions, with POM:ligand ratios ranging from 1:3 to 1:1. Two important features of the Keggin core dictate the nature of the final product: its charge related to the valence of the capping ion and the protonation states and also the coordination adopted by the capping ion. The synthesis of the materials described in this paper proves that a large family of original extended frameworks can be isolated, even though no stable porous materials have been obtained so far, and the simulation results show that the materials built from the connection of an ε-Keggin inorganic building unit and rigid linkers can potentially exhibit very large pores. It is now the chemist's role to investigate the synthesis of such phases. We will adopt two strategies: at room temperature we will continue to develop the reactions of the $[\varepsilon\text{-}PMo_{12}O_{36}(OH)_4\text{-}\{La(H_2O)_4\}_4]^{5+}$ polyoxocation with rigid polycarboxylates. We also are planning to investigate the replacement of lanthanum ions by rare-earth cations with smaller coordination numbers, such as Yb^{3+}. These rare-earth centres would be bound to a lower number of water molecules and the stability of the framework could therefore be improved. The second strategy will take advantage of hydrothermal conditions for the synthesis of porous materials with the aim of obtaining phases close to the simulated ones. The ε-Keggin core capped with transition metal cations (Fe^{III}, Ru^{III}, Mn^{III},...) will be generated in situ in the presence of O- or N-donor ligands. Furthermore, as demonstrated by recent results from our group, even if no single crystals are isolated and provided the X-ray powder pattern is of suitable quality, simulation combined with X-ray powder diffraction could allow us to determine the structure of these hybrids. Finally, the incorporation of POMs into hybrid organic–inorganic materials could lead to interesting applications. Indeed, these solids could combine the properties of POMs with those of porous materials, thereby opening-up a new perspective in the field of catalysis by POM-based compounds.

Experimental Section

General: All chemicals were used as purchased without purification. Elemental analysis was performed by the Service Central d'Analyse of CNRS 69390 Vernaison France. Infrared spectra were recorded with an IRFT Magna 550 Nicolet spectrophotometer at 0.5 cm^{-1} resolution, using the technique of pressed KBr pellets. X-ray powder diffraction data were collected with a Siemens D5000 diffractometer equipped with Cu-K_α radiation. The BET surface area analysis was performed with a Micrometrics ASP200 porosimeter. TGA experiments were performed under air (5°C/min) using a TA Instrument type 2050 analyzer apparatus.

Synthesis of $Na(C_{10}H_{10}N_2)[\varepsilon\text{-}PMo_{12}O_{40}Zn_4(H_2O)_2(C_{10}H_8N_2)_3]\cdot 10H_2O$ (1): A mixture of $Na_2MoO_4\cdot 2H_2O$ (0.47 g, 1.94 mmol), Mo (0.030 g, 0.31 mmol), $Zn(OOCCH_3)_2$ (0.16 g, 0.73 mmol), 4 M H_3PO_4 (46 μL, 0.18 mmol), 4,4′-bipyridine (0.06 g, 0.38 mmol) and water (5 mL; pH adjusted to 6.5 with 1 M NaOH) was sealed in a Teflon-lined reactor which was kept at 180 °C for 60 h. Black parallelepipedic crystals for single-crystal X-ray diffraction were hand selected from a product mixture. Crystals for elemental analysis were isolated by decantation after sonication and washed with EtOH (0.200 g, 36% yield in crystals, based on Mo). IR (KBr pellets): $\tilde{\nu}$ = 1541 s, 1505 s, 1409 s, 1299 w, 1018 w, 961 m, 934 s, 838 w, 815 m, 772 s, 754 s, 699 w, 599 s, 514 w cm^{-1}. $C_{40}H_{58}Mo_{12}N_8NaO_{52}PZn_4$ (2949.7): calcd. C 16.29, Mo 39.03, N 3.80, Na 0.78, P 1.05, Zn 8.87; found C 13.26, Mo 38.93, N 3.06, Na 1.04, P 1.05, Zn 10.75.

Synthesis of $[\varepsilon\text{-}PMo_{12}O_{35}(OH)_5La_4(C_8H_4O_4)_3]\cdot 41H_2O$ (2): $[\varepsilon\text{-}PMo_{12}O_{36}(OH)_4\{La(H_2O)_{2.5}Cl_{1.25}\}_4]\cdot 27H_2O$ (0.100 g, 3.2×10^{-5} mol) was dissolved in CH_3OH (5 mL). A solution of 6×10^{-3} M terephthalic acid (16 mL, 9.6 10^{-5} mol) adjusted to pH 6.0 was then added dropwise. The resulting microcrystalline burgundy powder (0.100 g, yield 86.5% based on molybdenum) was filtered and washed with H_2O and EtOH. IR (KBr pellets): $\tilde{\nu}$ = 1639 s, 1541 s, 1505 m, 1409 s, 1299 w, 961 m, 934 s, 838 w, 815 m, 772 m, 754 s, 699 w, 599 m, 514 m cm^{-1}. $C_{24}H_{99}La_4Mo_{12}O_{93}P$ (3613.88): calcd. C 7.98, La 15.37, Mo 31.85, P 0.86; found C 8.41, La 15.25, Mo 31.37, P 0.90.

Synthesis of $[\varepsilon\text{-}PMo_{12}O_{35}(OH)_5\{La(H_2O)_3(C_9H_3O_6)_{0.5}\}_4]\cdot 44H_2O$ (3): Crystals were obtained by slow evaporation of a solution of $[\varepsilon\text{-}PMo_{12}O_{36}(OH)_4\{La(H_2O)_{2.5}Cl_{1.25}\}_4]\cdot 27H_2O$ (0.050 g, 1.6×10^{-5} mol) dissolved in CH_3OH (5 mL) to which a 10^{-2} M trimesic acid solution (1.6 mL, 1.6×10^{-5} mol), adjusted to pH 3.9 with 1 M NaOH, was added. After two days red parallelepipedic single crystals of **3** (14 mg, yield 28% based on Mo) were filtered off. The crystals were left for two days in air in an open beaker to give **3** $_{subhyd}$. IR (KBr pellets): $\tilde{\nu}$ = 1611 s, 1554 s, 1435 s, 1369 s, 1263 w, 1113 w, 966 m, 932 s, 812 m, 758 s, 685 m, 602 m, 529 s cm^{-1}. $[\varepsilon\text{-}PMo_{12}O_{35}(OH)_5\{La(H_2O)_3(C_9H_3O_6)_{0.5}\}_4]\cdot 27H_2O$ ($C_{18}H_{89}La_4Mo_{12}O_{91}P$, 3499.7): calcd. C 6.17, La 15.88, Mo 32.90, P 0.89; found C 6.32, La 15.90, Mo 32.75, P 0.87.

Synthesis of $[\varepsilon\text{-}PMo_{12}O_{37}(OH)_3\{La(H_2O)_4\}_4(C_{10}H_2O_8)]\cdot 24H_2O$ (4): Single crystals were obtained by slow evaporation of a 4 mL solution of $[\varepsilon\text{-}PMo_{12}O_{36}(OH)_4\{La(H_2O)_{2.5}Cl_{1.25}\}_4]\cdot 27H_2O$ (0.020 g, 0.65×10^{-5} mol) to which a 5×10^{-3} M pyromellitic acid solution (1.3 mL, 0.65×10^{-5} mol) was added. After a few days red parallelepipedic crystals were collected by filtration (0.016 g, yield 75% based on molybdenum). IR (KBr pellets): $\tilde{\nu}$ = 1625 s, 1545 s, 1492 m, 1433 m, 1385 s, 1328 w, 1141 w, 966 m, 932 s, 812 m, 758 s, 685 m, 602 m, 529 s cm^{-1}. $C_{10}H_{77}La_4Mo_{12}O_{84}P$ (3279.6): calcd. C 3.66, La 16.94, Mo 35.10, P 0.94; found C 4.09, La 16.61, Mo 34.95, P 0.91.

X-ray Crystallography: Intensity data collection was carried out with a Siemens SMART three-circle diffractometer equipped with a CCD detector using monochromatic Mo-K_α radiation (λ = 0.71073 Å). The absorption correction was based on multiple and symmetry-equivalent reflections in the data set using the SADABS program[20] based on the method of Blessing.[21] The structure was solved by direct methods and refined by full-matrix least-squares

Table 3. X-ray crystallographic data.

	1	**3**	**4**
Formula	$C_{40}H_{58}Mo_{12}N_8NaO_{52}PZn_4$	$C_{18}H_{123}La_4Mo_{12}O_{108}P$	$C_{10}H_{77}La_4Mo_{12}O_{84}P$
Mol. mass	2949.74	3806.00	3279.56
Crystal system	monoclinic	orthorhombic	triclinic
Space group	$P2_1/m$	$P2_12_12$	$P\bar{1}$
Flack parameter		–0.020(17)	
Z	2	2	2
T [K]	296	296	296
λ [Å]	0.71073	0.71073	0.71073
a [Å]	11.6693(2)	20.5144(3)	12.3192(2)
b [Å]	17.7590(4)	21.7012(4)	12.3654(2)
c [Å]	17.2028(1)	12.1655(1)	25.1114(4)
V [Å^3]	3421.1(1)	5415.9(1)	3774.4(1)
$\rho_{calcd.}$ [g cm^{-3}]	2.724	2.346	2.866
μ [mm^{-1}]	3.624	3.021	4.287
Reflections collected	18313	38147	17178
Unique reflections (R_{int})	6235 (0.1425)	14089 (0.0656)	10642 (0.0784)
Refined parameters	432	584	985
$R_1(F_o)$[a]	0.0815	0.0544	0.0663
$wR_2(F_o^2)$[a]	0.1810	0.1037	0.1434

[a] $R_1 = \frac{\Sigma||F_o|-|F_c||}{\Sigma|F_c|}$; [b] $wR_2 = \sqrt{\frac{\Sigma w(F_o^2-F_c^2)^2}{\Sigma w(F_o^2)^2}}$ with $\frac{1}{w} = \sigma^2F_o^2 + aP^2 + bP$ and $P = \frac{F_o^2+2F_c^2}{3}$,

a = 0.0983, b = 0 for **1**; a = 0.0528, b = 0 for **3**; a = 0.0732, b = 0 for **4**.

using the SHELX-TL package.[22] Crystallographic data are given in Table 3. Selected bond lengths are listed in Tables 1 and 2.

CCDC-262218, -244419 and -262219 contain the crystallographic data for **1**, **3** and **4**, respectively. These data can be obtained free of charge from The Crystallographic Data Centre via www.ccdc.cam.ac.uk/data_request/cif.

[1] a) S. Kitagawa, R. Kitaura, S.-I. Noro, *Angew. Chem. Int. Ed.* **2004**, *43*, 2334; b) S. L. James, *Chem. Soc. Rev.* **2003**, *32*, 276.

[2] C. N. R. Rao, S. Natarajan, R. Vaidhyanathan, *Angew. Chem. Int. Ed.* **2004**, *43*, 1466.

[3] G. Férey, *Chem. Mater.* **2001**, *13*, 3084.

[4] M. Eddaoudi, J. Kim, N. L. Rosi, D. Vodak, J. B. Watcher, M. O'Keeffe, O. M. Yaghi, *Science* **2002**, *295*, 469.

[5] a) G. Férey, *J. Solid State Chem.* **2000**, *152*, 37; b) L. Beitone, C. Huguenard, M. Henry, F. Taulelle, T. Loiseau, G. Férey, *J. Am. Chem. Soc.* **2003**, *125*, 9102.

[6] P. Mialane, A. Dolbecq, L. Lisnard, A. Mallard, J. Marrot, F. Sécheresse, *Angew. Chem. Int. Ed.* **2002**, *41*, 2398.

[7] a) A. Müller, C. Beugholt, P. Kögerler, H. Bögge, S. Bud'ko, M. Luban, *Inorg. Chem.* **2000**, *39*, 5176; b) C. Lei, J.-G. Mao, Y.-Q. Sun, J.-L. Song, *Inorg. Chem.* **2004**, *43*, 1964.

[8] A. Dolbecq, P. Mialane, L. Lisnard, J. Marrot, F. Sécheresse, *Chem. Eur. J.* **2003**, *9*, 2914.

[9] N. E. Brese, M. O'Keeffe, *Acta Crystallogr. Sect. B* **1991**, *47*, 192.

[10] a) T. J. Prior, M. J. Rosseinsky, *Chem. Commun.* **2001**, 495; b) J.-C. Dai, X.-T. Wu, Z.-Y. Fu, C.-P. Cui, S.-M. Hu, N.-X. Du, L.-M. Wu, H.-H. Zhang, R.-Q. Sun, *Inorg. Chem.* **2002**, *41*, 1391.

[11] J. M. Poblet, X. López, C. Bo, *Chem. Soc. Rev.* **2003**, *32*, 297.

[12] Crystal data of $\mathbf{3}_{\mathbf{subhyd}}$ determined by simulation: orthorhombic space group $P2_12_12$ with a = 17.69, b = 21.48, c = 12.50 Å; V = 4750.4 Å^3.

[13] a) C. Mellot-Draznieks, J. M. Newsam, A. M. Gorman, C. M. Freeman, G. Férey, *Angew. Chem. Int. Ed.* **2000**, *39*, 2270; b) C. Mellot-Draznieks, S. Girard, G. Férey, *J. Am. Chem. Soc.* **2002**, *124*, 15326; c) C. Mellot-Draznieks, G. Férey, C. Schön, Z. Cancarevic, M. Jansen, *Chem. Eur. J.* **2002**, *8*, 4102.

[14] a) C. Mellot-Draznieks, J. Dutour, G. Férey, *Angew. Chem. Int. Ed.* **2004**, *43*, 6290; b) G. Férey, C. Serre, C. Mellot-Draznieks, F. Millange, S. Surblé, J. Dutour, I. Margiolaki, *Angew. Chem. Int. Ed.* **2004**, *43*, 6296; c) C. Serre, F. Millange, S. Surblé, G. Férey, *Angew. Chem. Int. Ed.* **2004**, *43*, 6285.

[15] C. Baerlocher, W. M. Meier, D. H. Olson, *Atlas of Zeolite Framework Types*, *5th revised edition*, Elsevier, Amsterdam, **2001**, and http://www.iza-structure.org/databases/.

[16] M. O'Keeffe, M. Eddaoudi, H. Li, T. Reineke, O. M. Yaghi, *J. Solid State Chem.* **2000**, *152*, 3.

[17] A. K. Rappé, C. J. Casewit, K. S. Colwell, W. A. Goddart III, W. M. Skiff, *J. Am. Chem. Soc.* **1992**, *114*, 10024.

[18] A. K. Rappé, W. A. Goddart III, *J. Phys. Chem. B* **1991**, *95*, 3358.

[19] Cerius2 Program suite from Accelrys, San Diego, USA, and Cambridge, UK.

[20] G. M. Sheldrick, *SADABS*; *program for scaling and correction of area detector data*, University of Göttingen, Göttingen, Germany, **1997**.

[21] R. Blessing, *Acta Crystallogr. Sect. A* **1995**, *51*, 33.

[22] a) G. M. Sheldrick, *Acta Crystallogr. Sect. A* **1990**, *46*, 467; G. M. Sheldrick, SHELX-TL version 5.03, Software Package for the Crystal Structure Determination, Siemens Analytical X-ray Instrument Division: Madison, WI (USA), **1994**.

Received: March 17, 2005
Published Online: June 28, 2005

